Final Draft
of the original manuscript:

Goebel, J.; Reimann, M.; Norman, A.; dos Santos, J.F.:
Semi-stationary shoulder bobbin tool friction stir welding of AA2198-T851

In: Journal of Materials Processing Technology (2017) Elsevier

DOI: 10.1016/j.jmatprotec.2017.02.011

Semi-stationary shoulder bobbin tool friction stir welding of AA2198-T851

Authors:

Jannik Goebel[a], Martin Reimann[a], Andrew Norman[b], Jorge F. dos Santos[a]

Affiliations:

[a] Helmholtz-Zentrum Geesthacht, Institute of Materials Research, Materials Mechanics, Solid State Joining Processes Department, Max-Planck-Str. 1, 21502 Geesthacht, Germany

[b] ESA, European Space Agency, Product Assurance and Safety Department, Materials Technology Section, Noordwijk, The Netherlands

Corresponding author:

Jannik Goebel. Tel.: +49 4152 872068 Fax: +49 4152 2033 mail: jannik.goebel@hzg.de

Abstract

The aluminum lithium alloy AA2198-T851 has been bobbin tool friction stir welded using a tool concept with one stationary and one rotating shoulder. Defect free welds in 3mm thick sheet have been produced featuring a high quality surface finish on the stationary side. The macrostructure forms an asymmetrical shape with microstructural characteristics known from standard friction stir welding. Because of only one rotating side a material flow direction towards the stationary shoulder has been observed. A parameter survey shows that a weld pitch of one mm per rotation combined with high pressure between the shoulders lead to good results. Mechanical performance of 82 % of base metal ultimate tensile strength and 77 % of base metal hardness have been achieved. The fracture analysis indicates two competing fracture modes, one being in the heat affected zone and the other at the borderline of the stirred zone on the advancing side. The first mode forms due to thermal cycle influence, whereas the second location suffers from weak bonding as a result of the thermal cycle and experienced deformation.

Graphical abstract

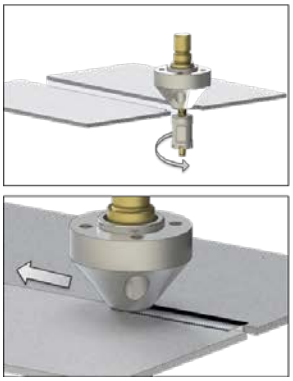

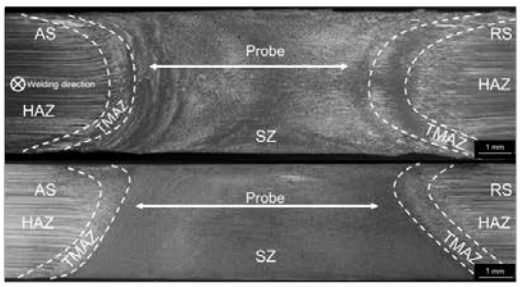

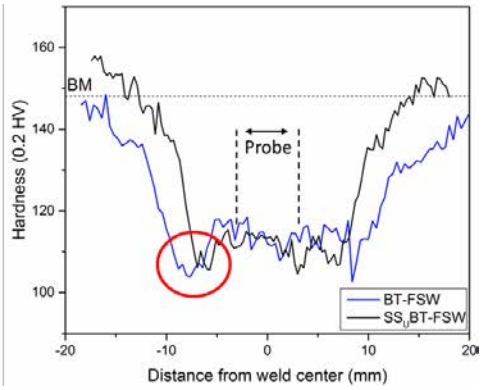

Highlights

- A comparative study was conducted between BT-FSW (bobbin tool) and semi-stationary BT-FSW.
- Flawless welds were achieved in both cases with superior surface finish in the stationary variant.
- The macrostructure of the stationary variant changed to an asymmetrical shape and material flow.
- Higher mechanical performance was determined, the point of lowest mechanical performance was correlated with a most unfavorable precipitation state.

Keywords

bobbin tool; friction stir welding; stationary shoulder; aluminum; microstructure; girth welding

1 Introduction

Al-Li alloys were first cast in the 1920s. As the lightest metallic element, lithium reduces the density by 3% and enhances the elastic modulus by 6% for every added weight % Li. Therefore, Al-Cu-Li alloys are of special interest when high specific strength and modulus materials are required and can consequently be found in many aeronautical and aerospace applications. Wanhill et al. summarized some examples like the floor or lower wing structure of the Airbus A380 (2013c). AA2198 is a representative of the third and most modern generation of the aluminum-lithium alloys and was used as for the SpaceX Falcon9 first and second stage skin materials (2010b).

High strength aluminum alloys, often heat treated, exhibit unacceptable defects such as hot cracking when welded above the solidification temperature. Mishra et al. (2005a) reviewed the friction stir welding process and stated these effects are especially present in high strength Al-alloys. The solid-state nature means that friction stir welding (FSW) is especially suited to welding materials suffering from high heat impact.

Bobbin tool friction stir welding (BT–FSW) is a variant of solid-state friction stir welding. The principle of FSW, which forms a strong joint by the intermixing of plasticized material, is identical in BT–FSW, with the difference that the frictional heat is applied from both sides, as the BT–FSW consists of two rotating shoulders connected by the probe. In addition to the often cited advantages compared to fusion welding, such as lower heat input, higher performance or improved weldability, as summarized by Cam et al. (2014a), by the bobbin tool variant. Additionally, no anvil is needed. It is therefore particularly suitable for closed structures such as pipes or hollow extrusions. Since full penetration is guaranteed, common defects such as root flaws or lack of penetration sometimes reported in standard FSW are avoided. However, the increasing flexibility results in a lack of stiffness and simplicity of the system, making it harder to achieve industrial acceptance. A further drawback is the remaining exit hole at the end of the weld, which is usually closed in a subsequent process, such as the recently proposed keyhole closure technique using refill friction stir spot welding reported by Reimann et al. (2016). Still, increasing numbers of publications in the field of BT–FSW in recent years are proof of growing interest in this technology. While most investigations focus on the 6xxx series, only a few studies have been conducted on high strength aluminum 2xxx series. Schneider et al. (1991) investigated the interactions of bulging, grain refinement and the strength of welds in AA2195-T8, and Skinner et al. (2003b) studied process characteristics, configuration and mechanical properties. Wang et al. (2015c) demonstrated the BT–FSW process in AA2198-T851. The material was successfully welded, and the microstructural analysis revealed a correlation between the joint line remnant, a line of oxide particles originating from the butting surface and the rotational speed. In 2006 a tool concept known as a stationary shoulder FSW (SSFSW) was presented by Widener et al. (2006). In this variant, the shoulder is decoupled from the rotation of the probe to be stationary, and the temperature needed to generate plasticity is produced by the probe. Initially developed for welding high temperature, low conductivity materials such as titanium, this concept was also applied to aluminum alloys. Promising results have been achieved welding different aluminum alloys by Liu et al. (2013a) who used an external

non-rotational shoulder in AA2219 or by Buffa et al. (2010a) who welded first corner joints and proved his findings by using a thermal model. While some findings have been presented at conferences, only a few extensive studies are available. A first, systematic investigation to compare FSW to SSFSW was published by Wu et al. (2015d). Although using similar tool geometries, the welds produced in AA7050 were difficult to compare using common methods due to a lack of overlap of the process windows. As a solution, Wu compared the optimum welding parameters resulting from the power-rotation curve of both processes. Employing this method, 30% less heat input was reported when the shoulder was kept stationary. Consequently, the macrostructure changed to a narrower, parallel appearance and performed better in terms of mechanical properties. A smooth and less rough surface was attributed to the ironing effect of the sliding shoulder.

In recent years, the stationary shoulder approach was developed to improve the BT–FSW process to reduce the total heat required input. Although the full stationary BT–FSW process has had remarkable challenges in terms of tool material and design, the use of partly stationary tool concept proved the concept. In 2015 Scupin (2015b) achieved welds with an stationary upper shoulder in BT–FSW in AA6082 T4, reaching mechanical properties close to the base material.

In consistency with common terminology in friction stir welding, the term bobbin tool (BT–FSW) refers to a two shoulder and one probe tool while self-reacting bobbin tool (SRBT–FSW) is referred to a force controlled process variant which allows the shoulder distance to vary (“to react”). Stationary shoulder FSW (SSFSW) consists of one stationary shoulder and one rotating probe, consequently stationary shoulder bobbin tool (SSBT–FSW) features two stationary shoulders and one rotating probe. If semi-stationary tools are used the stationary part will be identified by ‘up’ or ‘low’ for the respective shoulder. A semi-stationary bobbin tool with a static upper shoulder will be named as SS_UBT–FSW and a semi-stationary bobbin tool with a static lower shoulder is named SS_LBT–FSW. In this work, SS_UBT–FSW is presented.

In this work, a semi-stationary shoulder bobbin tool FSW is firstly employed to produce high-quality welds with superior surface finishes and mechanical properties in AA2198–T851. The macrostructure and flaw distribution are presented and compared to a standard BT–FSW joint with two rotating shoulders. SS_UBT–FSW specimens were produced and analyzed for their hardness and tensile characteristics. Furthermore, thermal cycle measurements were carried out to investigate the heat input in the stationary shoulder variant and establish its effect in the resulting microstructure and the mechanical performance.

2 Materials and Methods

2.1 Aluminum alloy 2198–T851

The aluminum-lithium alloy 2198 was utilized in T851 temper. This special multistage thermomechanical processing consists of solution heat treatment, stress-relieving by stretching and subsequent artificially ageing. The chemical composition is listed in Table 1 (2009). The material has a density of 2.69 g/cc and an elastic modulus of 75 GPa. AA2198 was developed as third generation aluminum-lithium alloy and patented in the year 1995 (1995). The base material has been cut to produce samples measuring 300x75x3 mm for SSUBT–FSW experiments and 300x75x4.2 mm for BT–FSW.

Table 1: Chemical composition of the alloy AA2198

Cu	Li	Zn	Mg	Mn	Zr	Fe	Al
3.2	1.0	0.014	0.31	0.005	0.076	0.046	Rem.

2.2 Experimental procedure

In order to compare this process variant with the standard BT-FSW, a mutual factor must be determined. As the working process windows for the standard and the stationary variants do not overlap and the welding parameters play a key role in the joint formation, a direct comparison is difficult to make. Wu et al. (2015d) faced similar challenges when investigating stationary shoulder FSW versus standard FSW, and decided to compare the results with respect to the optimum parameters of the respective process window. Thus, the best working parameters for each variant were used to demonstrate and compare the principles of both processes.

All welds were produced on a five-axis parallel kinematic robot system (PKM T805) equipped with a custom designed BT–FSW spindle. The tools consisted of a 7 mm, featured probe and two 15 mm diameter shoulders. The probe was manufactured from the nickel-cobalt alloy MP159 with inclined features. The shoulder material was a molybdenum-vanadium hot work tool steel (X38CrMoV5-1). The rotating shoulder had symmetrically scrolled features, whereas the stationary shoulder was featureless. Welding parameters were adjusted to 400 RPM at a transverse speed of 500 mm/min. The process runs in self-reacting mode at 5000 N allowing the gap width to vary. For the standard BT–FSW welds, the following parameters were employed: 600 RPM and 200 mm/min at 2500 N. Standard BT–FSW welding was performed using a 4.2 mm sheet. Both parameter sets represented conditions where sound welds could be produced in a reproducible manner. To analyze the influence of the process parameters of the stationary shoulder variant on the tensile characteristics, the rotational speed was varied from 400 to 600

RPM and the gap force from 4000 N to 5000 N (the force transferred by both shoulders on the base material), whereas the weld pitch was held constant at one rotation per mm.

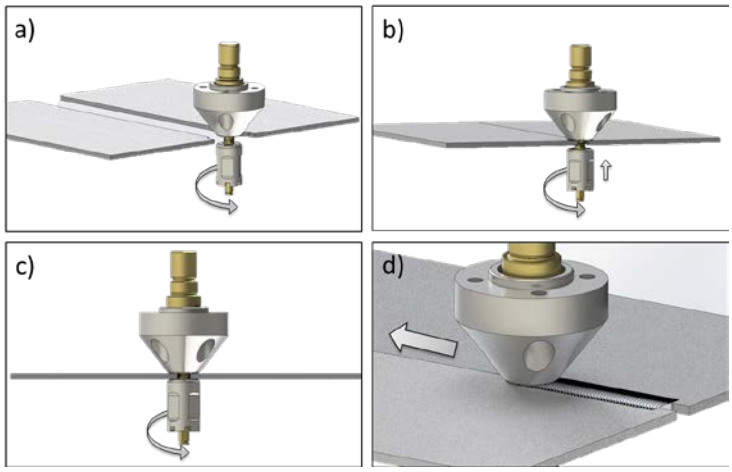

Figure 1 SS_UBT–FSW welding process.

Figure 1 illustrates the SS_UBT–FSW process with the tool penetrating the workpieces and joining the two sheets in a butt joint configuration. The lower shoulder and the probe were fixed and in constant rotation, whereas the upper shoulder was held stationary by a decoupling system. The welding process was run in the force controlled mode and is shown in Figure 1 a)–d). After rotation is started, the tool approaches the workpiece where both shoulders move to touch the substrate. Once the desired force between the shoulders is reached, the tool begins to move forward and forms the weld.

2.3 Test and Analysis

To record the thermal history in the weld during the SS_UBT–FSW process, four K–type thermocouples were embedded in the aluminum sheets at mid-thickness at distances of 5, 8.5, 10 and 13.5 mm from the weld center. The temperature measurements were taken after 100 mm of welding when the thermal condition is assumed to have stabilized.

For microstructural analysis, samples were sectioned perpendicular to the welding direction and prepared using standard metallographic specimen preparation procedures including flat grinding and finish polishing. The microstructure analysis was performed using polarized light microscopy. The polished samples were etched using a three vol.% solution of HBF4 known as BARKER solution at 22 V for 90 seconds. The grain dimension was measured employing LEICA software and following the ASTM E112-13 standard. Topographic mapping was performed using a Keyence Color 3D laser microscope VK-9700.

Prior to testing, all specimens were left at room temperature for four weeks allowing any natural aging processes to stabilize. For mechanical testing, samples were machined into a dog-bone shape with dimensions indicated in Figure 2. Tensile tests were carried out in a Zwick & Roell machine equipped with

a 100 kN load cell in accordance to ISO 6892-1:2009. Testing was performed perpendicular to the rolling direction with a speed of 1 mm/min. The hardness measurements were conducted on a Zwick Vickers hardness tester (LECO, type M-400-H) in accordance with ISO 6507-1:2005 by applying 200 grams for 10 s. The hardness measurement was performed at mid thickness, and the distance between the indentations was 400 µm.

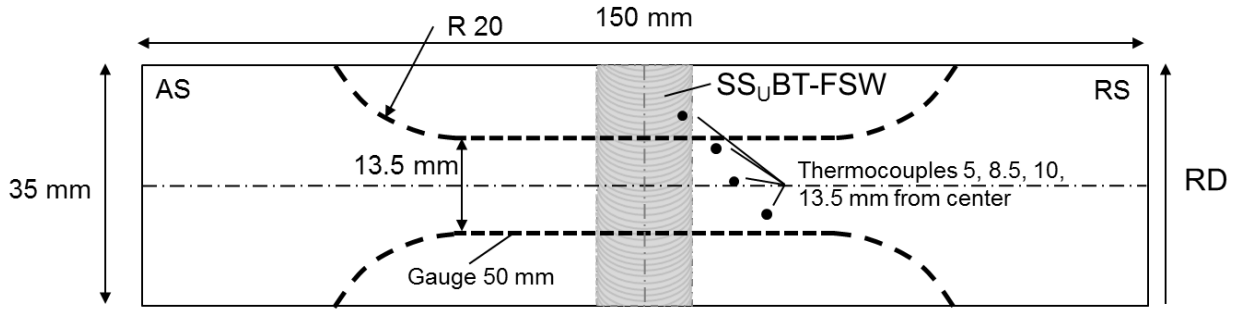

Figure 2 Dimensions of tensile testing coupons and thermocouple positions.

3 Results & Discussion

3.1 Stationary shoulder in BT–FSW

Two main observations were made when comparing SS_UBT–FSW to standard BT–FSW. First, it was noted that due to the sliding of the stationary shoulder, the process is more stable. This results in less intense planar peak forces perpendicular to the welding direction. It is assumed that the less softened material on the stationary side stabilized the probe due to its higher resistance. Hence, the workpiece itself guides the tool. This is especially attractive when welds are produced using a system where flexibility is increased at the cost of stiffness, such as for robotic arms.

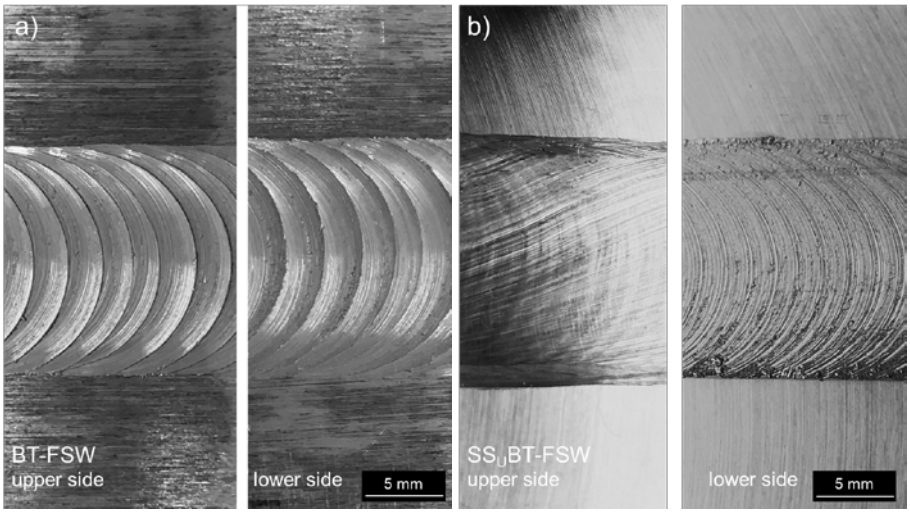

Figure 3 Surface appearance: a) standard BT–FSW and b) semi-stationary bobbin tool friction stir welds.

Another positive observation is the ironing effect shown in Figure 3 b). This effect describes the smoothing of the weld surface due to the sliding, stationary shoulder. The characteristic semicircular tool marks resulting from the rotating shoulder are flatted to a surface finish that is similar to and sometimes better than that of the pristine material. The stationary shoulder acts as a moving anvil plate and compresses the material, which has been previously plasticized by the probe. “Speed cracks”, a phenomena known from extruding aluminum, resulting from overheated material sticking to the tool surface were not observed in the present study. Surface topography measurements from the BT–FSW and SS_UBT–FSW joints shown in Figure 3 are presented in Figure 4. By holding the shoulder stationary, the surface roughness could be improved by as much as a factor of five. Still, small-scale semicircular marks are detectable for the SS_UBT–FSW, confirming these marks are produced by the probe induced material flow. Although the exact formation mechanism of these marks is uncertain, the distance between them was identified to represent the forward movement of the tool over one rotation. Krishnan et al. (2002b) attributed this phenomena in 6061 and 7075 friction stir welds to geometrical effects and the formation to the extrusion of the material around the probe.

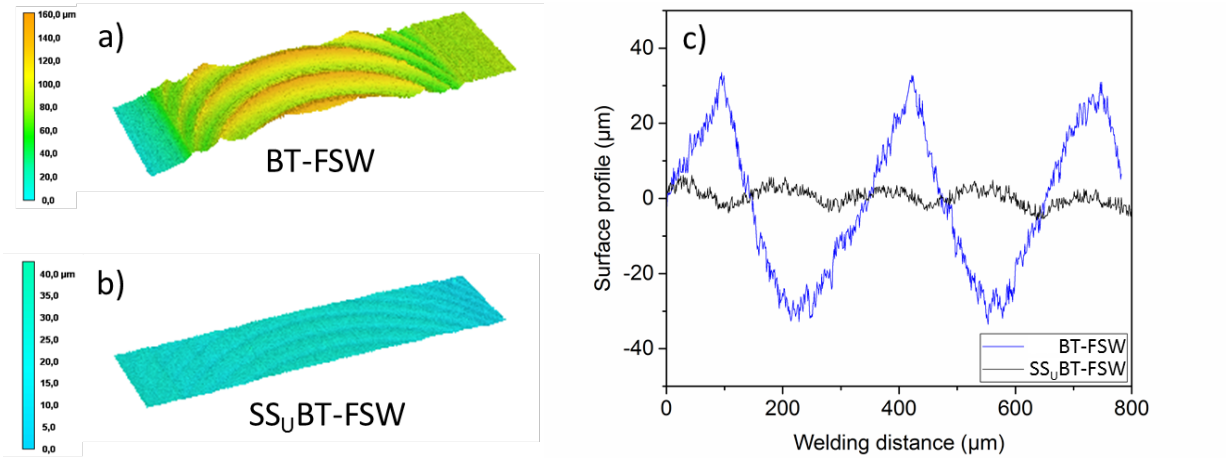

Figure 4: Surface topography: a) of the standard BT–FSW, b) of the semi-stationary and c) in comparison.

3.2 Microstructural features

The macrographs of cross sections of the BT–FSW and SS_UBT–FSW welds are shown in Figure 5. Welds were obtained with no defects for both cases. Compared to a standard BT–FSW macrograph, which are described as hourglass shape, the SS_UBT–FSW weld features an asymmetrical shape widening up towards the rotating, lower shoulder. Still, an hourglass shape characteristic of having two shoulders is visible.

The macrostructure reveals the typical welding zones consisting of a centered stirred zone (SZ), which is flanked by the thermo-mechanically affected zone (TMAZ). This is in turn connected to the heat affected zone (HAZ), which ends in the base material (BM) for both welding variants.

The SZ experienced the highest shear rates and peak temperatures. It consists of fully recrystallized, fine grains with an average grain diameter of six µm in both the BT–FSW and SS_UBT–FSW process variants. No variations of the grain size were measured towards the stationary shoulder. The probe diameter was 7 mm, and the mid-width of the SZ is extended by approximately 10% to the retreating side (RS) of the weld. As investigated by Colligan (1999), who applied a steel ball tracer to analyze the material flow in aluminum FSW joints, material extrusion around the probe plays a significant role in the SZ formation. The SZ is widened to the RS due to the extrusion of hot, sheared material around the probe.

The TMAZ is the transition zone from the SZ to the HAZ and experiences medium strain rates and high temperatures. The grains are slightly elongated and deformed vertically in both welding variants. The interface to the SZ is sharper on the advancing side (AS) and appears more defused on the RS. This is a characteristic feature observed in all FSW. Cabibbo et al. (2007) did a microstructural investigation on FSW AA6056 and found higher strain rate and temperature gradients on the AS caused by the greater material flow on RS, as well as the high shearing from the probe. The width of the TMAZ may vary with

tool dimensions and parameter settings and was not significantly influences by the stationary shoulder variant.

The HAZ is affected by the thermal cycle and experiences no plastic deformation. The grain size corresponds to the grains of the unaffected base material for both process variants, and the pancake shaped grains resulting from the rolling process were measured to be 11 x 4 µm.

In SS_UBT–FSW welds, as shown in Figure 5 b), the asymmetric shape of the SZ opens up towards the lower surface. At the lower side, the SZ width equals the shoulder diameter due to the shoulder influenced rotation. Towards the upper surface the SZ widens up as well but to a much less extend. This is due to the missing stirring effect of the upper stationary shoulder. The stationary shoulder reduces the total area of the SZ and the overall width of the affected material due to decreased mechanical and thermal influence. This is assumed to have beneficial consequences with regard to the precipitation state, see chapter 3.4.

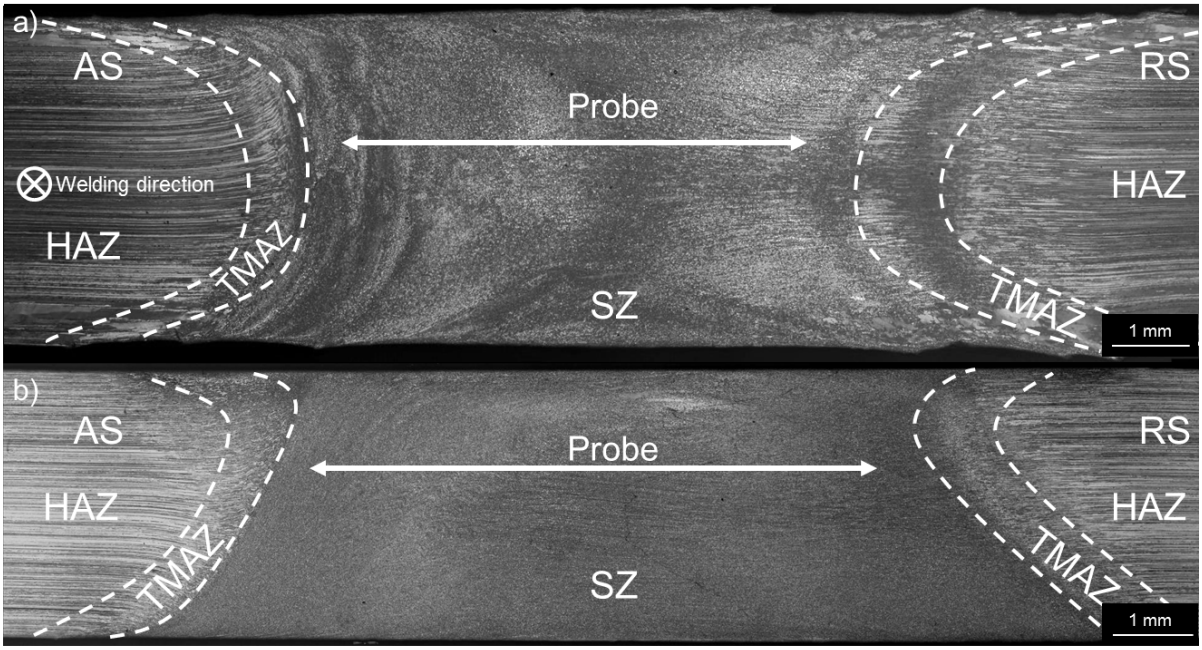

Figure 5 Macrographs of BT–FSW (a) and SS_UBT–FSW (b) welds.

3.3 Characteristic aspects of SS_UBT–FSW material flow

In FSW processes, the substrate material is moved from the RS to the AS due to the rotational movement of the probe. Sheared material from the AS accumulates with the material in front of the moving tool that is displaced by the probe movement and extruded via the RS to the back of the probe. Behind the probe, the plasticized material refills the space left by the moving probe, establishing metallic bonds on the AS. Chen et al. (2008) confirmed this by looking on the trailing side of a stable FSW process in AA5083. The detaching of the material from the probe was attributed to the high velocity ratios from inner to outer shear layer. The critical region to be reinforced is the surface on the AS, where the base material was sheared

and refilled with plasticized material behind the probe, creating a sharp transition from the SZ to the TMAZ, as shown in Figure 6.

Volumetric flaws that appear due to inadequate parameters are most likely to occur at this interface and can be used as indicators of the apparent material flow. Typical volumetric flaws observed in FSW are reported on the AS due to insufficient material transport. In standard BT–FSW this 'wormhole'-like defect can be found at the mid-thickness, where both shoulder-induced material flows meet, as shown in Figure 6 a). Due to the asymmetrical character of the SS_UBT–FSW variant, these defects are forced upwards towards the stationary shoulder, as shown in Figure 6 b).

In Figure 6, the typical flaw location for both processes is shown with the indicated flow direction. In SS_UBT–FSW, a vertical material flow forms in the weld zone on the AS, which is caused by shoulder-induced movement as well as the threaded probe. The defects are identified by higher magnification as a lack of consolidation due to insufficient material flow, as shown in Figure 6. Possible reasons for this are excessively low temperatures and pressures. Volumetric defects resulting from non-optimal parameter settings will occur at the top surface and are easy to locate. These critical spots can be attributed to an insufficient material flow. Further parameter variations promoting material flow will lead to a flawless weld, as shown in Figure 5.

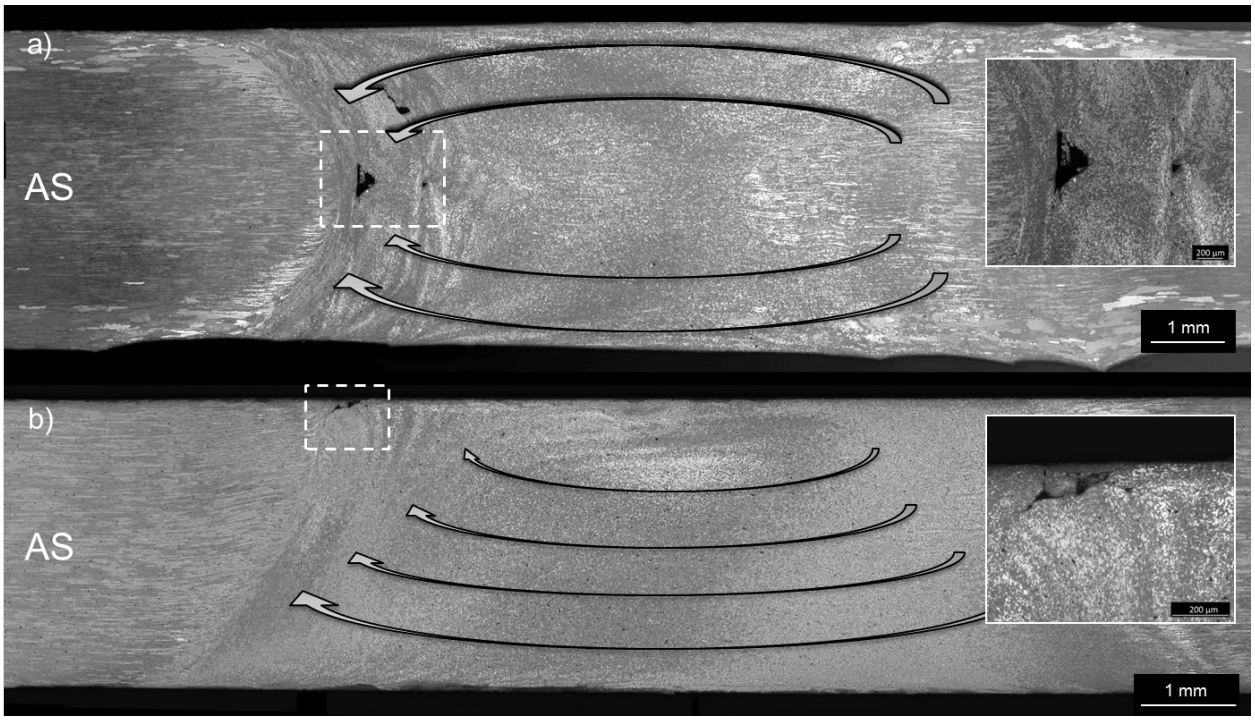

Figure 6 Material flow and volumetric critical locations in BT–FSW (a) and SS_UBT–FSW (b) welds.

3.4 Thermal cycle analysis in the SS$_U$BT–FSW

The thermal cycle measurements were carried out at various distances from the SZ. The size of the SZ varies with the process parameters and tool dimensions. Since minor variations in thermocouple measurements can have a significant effect on recorded thermal cycle, the exact final position after welding was determined ex-situ via metallographic methods.

The high force between the shoulders resulted in a measured torque of 38.9 Nm. Following the heat input relationship ($E = Torque \cdot 2\pi \cdot RPM/speed$), the heat input per unit length was calculated to be 219 kJ/m. Four thermocouple positions were used as indicated in Figure 2.

When the measured distances were referenced to the SZ borderline, the temperatures on the AS and the RS develop similarly. It is assumed that the heat generated in the SZ causes an even temperature distribution due to the high stirring effect. Starting from the SZ, the heat is assumed to propagate equally to both sides of the weld and into the base metal. When deformation influences are not present (e.g., in the HAZ) the heat transfer is purely dependent on the thermal properties of the substrate and the temperature difference. Therefore, the temperature distribution in the HAZ on both sides of the SZ should be similar.

In this study, no difference in temperature on the AS and RS could be measured. Nevertheless, preferred failure in the AS was evident in tensile fracture mode II. This would indicate a higher thermal impact in the AS. All of the tested samples with a flawless microstructure failed on the AS. Liu et al. (2003a) found that for the fracture behavior of FSW joints in AA2017-T3, high copper-containing aluminum alloys seem to be more susceptible to a weakening mechanism on the AS.

Figure 7 a) presents thermal cycles recorded at two locations on the AS of the weld. The curves show a high heating rate between 100°C and 300°C of approximately 130 K/s. The first peak temperature was measured at a distance of 1.6 mm from the SZ and was 446°C. The second thermocouple at a distance of 6 mm measured 0.6 s later exhibits a peak temperature of 299°C.

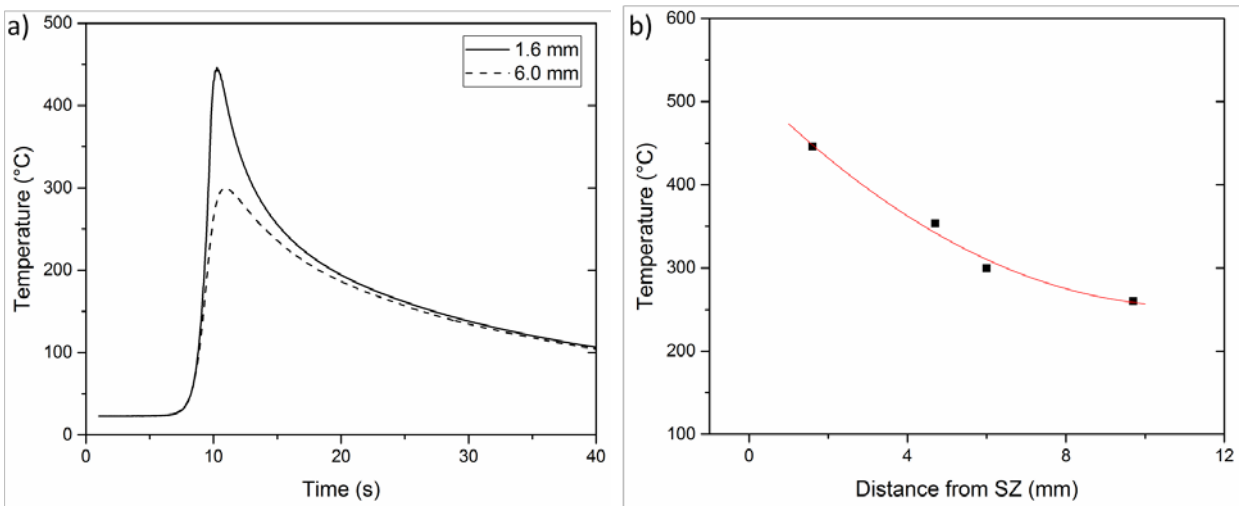

Figure 7 Temperature cycle (a) and maximal temperature distribution (b) in SS$_U$B-FSW.

In Figure 7 b), the four measuring positions were fitted polynomial to provide an impression of the peak temperature variation as a function of the distance to the center of the SZ. Extrapolating this model, the maximum temperature at the borderline to the SZ would approximately 519°C. Confirmed by Taylor et al. (2014b), who performed a microstructure mapping in the Al-Cu-Li alloy AA2050 using SAXS measurements, temperatures above 300°C start to coarsen and dissolve the T_1 precipitates, whereas no change was detected at small intervals for temperatures under 250°C. Above 400°C, almost no T_1 precipitates were detected.

3.5 Mechanical behavior of SS_UBT–FSW welds

The microhardness profiles of the SS_UBT–FSW and BT–FSW welds are presented in Figure 9. Both profiles display a W-shape, which has often been reported for high-strength, precipitation-hardened aluminum alloys. The hardness is sensitive to the metallurgical state. It is strongly assumed that variations in the microhardness in different regions of the FSW joints are associated with the evolution of precipitates in precipitate hardening aluminum alloys. Gao et al. (2015a) compared the different strengthening mechanisms between the welding zones in AA2198 FSW welds and found precipitations as main contributors in BM and HAZ while the SZ was predominantly strengthened by grain refinement.

The precipitation sequence in aluminum lithium is a complex system featuring aspects from both binary Al-Cu and Al-Li systems. The Al-Cu system contributes to the formation of GPI and GPII zones followed by θ′ (Al_2Cu) precipitates, whereas the Al-Li system promotes the formation of the δ′ (Al_3Li) precipitates. Consequent artificial aging of the ternary system will promote the formation of several phases of which the T_1 (Al_2CuLi) precipitate is the most important high strength precipitate. Other phases include the S(Al_2CuMg), T_2(Al_6Li_3Cu) or T_b($Al_{7.5}LiCu_4$) precipitates which can form depending on the alloy composition and processing conditions. The precipitation reaction for AA2198-T851 can be stated following the sequence summarized by Jo and Hirano (1987):

$$\alpha\ (SSS) \rightarrow GP\ zones \rightarrow GP\ zones + \delta' \rightarrow \theta'' + \theta' + \delta' \rightarrow \delta' + T_1 \rightarrow T_1.$$

The aim of the third-generation aluminum lithium alloys is to maximize the nucleation of the partially coherent equilibrium T1 phase. This phase is the most efficient strengthening phase but competes with the δ′ phase for the available lithium. High dense nucleation of T1 was achieved by increasing the dislocation density due to cold working prior to the final aging (T8) step as well as small additions of Ag and Mg. The amount of the main strengthening precipitate T1 is highest in the peak aged temper (T8); therefore, the BM exhibits the highest hardness of 149 $HV_{0.2}$.

Chen and Bhat (2002a) demonstrated the hardness variation as a function temperature and time in the similar Al-Cu-Li alloy 2195. Although the shortest isothermal treatment investigated is 36 seconds and therefore much longer than the welding processes analyzed in this study, a clear trend of softening can be seen when temperatures are above 250°C (~500F). Further, a time-temperature-precipitation diagram was presented which displays GP and δ′ phases being formed during natural aging at temperatures below 94°C (~200F). It is assumed that the material softens during the welding process due to dissolution of artificially aged precipitations above 200°C and hardens after welding at room temperature forming Co-clusters, GP zones and δ′ phases.

Starting from BM values at approximately 17.5 mm from the center of the weld, the hardness drops as the distance to the centerline decreases, see Figure 8. This softening effect is shifted to the center when one shoulder is hold stationary which can be seen in the hardness profile. It can be seen that the shape of the semi-stationary variant is narrower, which mirrors the narrow shape also seen in the macrostructure. The

HAZ becomes gradually softer due to the increasing influence of the high temperatures, which are assumed to cause partial dissolution of the strengthening precipitates. The weakest area of 104 $HV_{0.2}$ is located in the HAZ. The TMAZ is found from the increasing values, which reach a constant value of approximately 115 $HV_{0.2}$, indicating the beginning of the SZ. The SZ exhibits a relatively constant hardness of 115 $HV_{0.2}$, which corresponds to 77% of the BM values. While the shape is different the harness values are similar between the two process variants. In the SZ, the material is exposed to the highest temperatures, which were measured at above 450°C, see chapter 3.4. This is above dissolution temperature of the T1 precipitate and leads to a supersaturated solution predestined to natural aging processes. During the natural aging process, several hardening contributors are formed like co-clusters or precipitates like θ' or δ′ which were identified in natural aged (T3) Al-Cu-Li alloy by Zhang et al. (2014c) analyzing SAD pattern. The effect of strengthening due to natural aging processes can be observed when comparing the SZ hardness two hours after welding with its hardness after four weeks, compare Figure 8.

The point of lowest hardness in the HAZ is observed as most critical due to possible load concentrations and as the subsequent failure at this point. Gao et al. (2015a) presented a correlation between the tensile properties and the volume fraction of T1 phases in an FSW and quantified the contribution of the different strengthening mechanisms in a FSW weld. The main strengthening mechanisms in the BM, HAZ and TMAZ are precipitation hardening, whereas the SZ is also strengthened by grain refinement.

Following this assumption and that the stronger thermal influence closer to the weld center leads to the stronger dissolution of the T1 precipitates as well as re-strengthening during post-weld natural aging (δ′), the point of the lowest hardness is where the ratio between the formation of the natural aging phases and the dissolution of T1 precipitates is the lowest. The point of the lowest hardness is located in the HAZ where precipitation strengthening plays a key role. Here, solution softening (due to T1 dissolution) and precipitation strengthening (due formation of natural aging phases) mechanisms are in concurrence.

This point is an important characteristic for every weld, and the distance from the center depends on the tool dimensions and the heat input influenced by the process parameters. This point is approximately 1.3 mm further away from the center of the weld when comparing the semi-stationary to the standard variant. This correlates well with the distances measured in the macrostructure (Figure 5) where the SZ is found narrower.

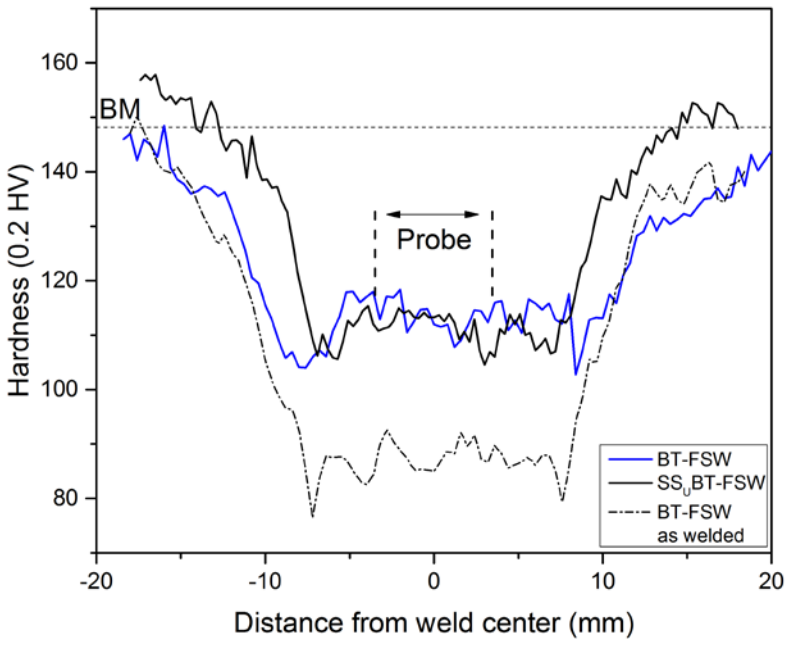

Figure 8 Microhardness profiles of the BT–FSW and SS_UBT–FSW welds.

The influence of SS_UBT–FSW process parameters on the ultimate tensile strength (UTS) is given in Figure 9. The base metal was tested confirming the literature data for the LT direction. Best parameters of the SS_UBT–FSW weld fractured at an UTS of 417 MPa with a yield strength (YS) of 285 MPa, which corresponds to 82% and 56% of the BM values, respectively. Other studies employing FSW in aluminum-lithium alloys in the T8 temper have shown efficiencies of approximately 70% (alloy 2195 (2005a) or alloy 2198 (2013b)). In a recent study, Wang et al. (2015c) employed BT–FSW to achieve an ultimate tensile strength of 379 MPa in 3.2 mm thick AA2198-T851 which was also achieved using the standard BT–FSW variant (Figure 9). It is therefore inferred that the stationary shoulder variant can diminish defect occurrence and increase the tensile strength.

We note that the gap force between the shoulders was the crucial parameter to achieve a flawless weld and corresponding high mechanical performance. This is due to the additional forging effort needed to transport the material through the whole thickness. A higher forging effort is implied by lowering the gap width. It is noted that welds exhibiting a UTS less than 375 MPa fractured in the SZ. These welds were not considered flawless, as the fracture was initiated from consolidation defects at the upper surface, as shown in chapter 3.3. Complete consolidation of the joint was found when the gap force was increased to 5000 N. The flawless welds failed in two types of fracture modes, which are presented in Figure 10.

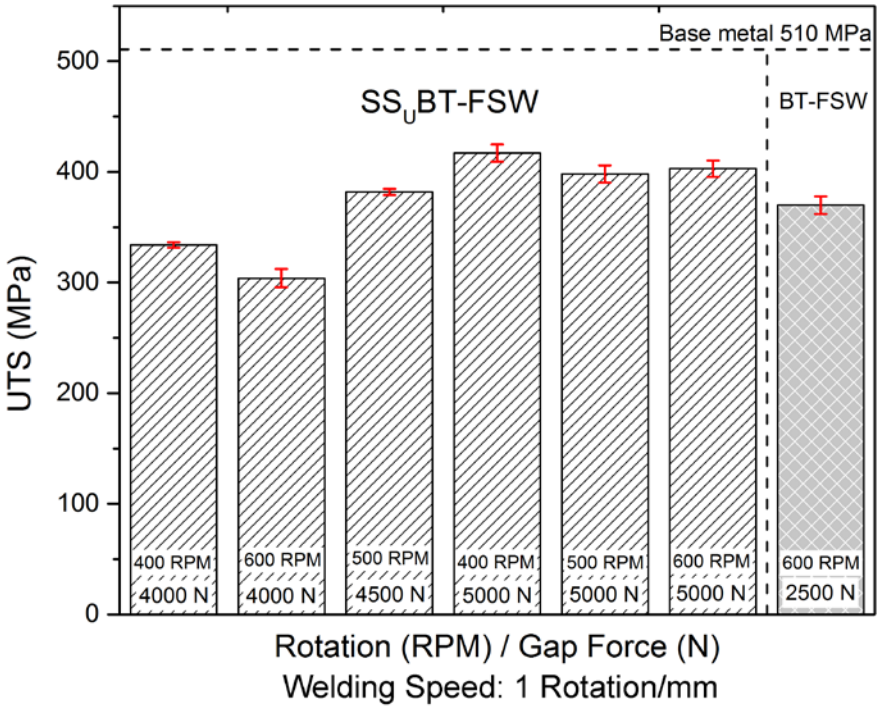

Figure 9 Tensile test results for the SS$_U$BT–FSW and BT–FSW specimens.

The flawless welds were subjected to tensile testing and fractured in two fracture modes. Fracture mode I shows a shear mode fracture on the AS of the SZ at the border of the TMAZ. The fracture path follows the border between the SZ and the TMAZ, which is at an almost 45° angle. The mode II fracture occurs in the HAZ and follows a 45° path. Fracturing in a shear mode well away from the SZ suggests softening due to thermal effects. Thus, the distance from the weld center correlates with the weakest point in the hardness distribution, as shown in Figure 8. Mode I fracture indicates a competing weakening mechanism located at the SZ-TMAZ border on the AS. This may be related to the high misorientation observed in the AS for FSW by Prangnell et al. (2005b). Further investigations are needed to understand this mechanism. The samples fractured in mode I and II in equal numbers.

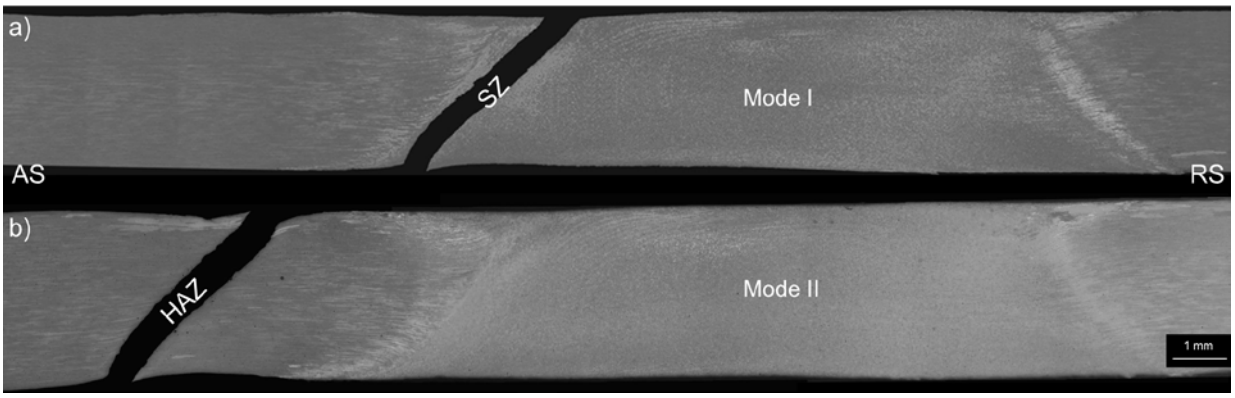

Figure 10 Fracture modes for SS$_U$BT–FSW: a) mode I in SZ, b) mode II in HAZ

Following the findings from chapter 3.4, the main precipitation state changes occur up to a distance of 6.5 mm from the SZ in the samples described in this work. The defined failure modes occur in regions where highest temperatures of 519°C were assumed (mode I) and temperatures of 350°C (mode II) were measured. The latter, mode II, occured at a distance of 6.0 - 7.6 mm where the thermal influence formed main precipitation state changes resulting in the lowest measured hardness.

4 Conclusions

1. The macrostructure exhibits an asymmetrical hourglass shape with characteristic zones known from FSW. A fine recrystallized layer is formed due to the sliding of the stationary shoulder.
2. The material flow indicates an upward flow leading to the distribution of volumetric defects close to the sheet surface on the AS when imperfect process parameters were used. This is considered advantageous, as defects are easily detected and are capable of being removed if necessary.
3. Flawless welds featuring a high surface finish on the stationary shoulder side were achieved featuring an ultimate tensile strength efficiency of 82%, a yield strength efficiency of 56% and a hardness efficiency of 77%. A weld pitch (rotation/mm) of one and high pressure between the shoulders led to the best results.
4. Two fracture modes located in the HAZ and at the borderline of the SZ/TMAZ were identified, indicating competing weakening mechanisms. The weakened HAZ location forms due to the thermal cycle influence, resulting in weak precipitation morphology, whereas the SZ/TMAZ location suffers from weak bonding as a result of the thermal cycle and deformation.

Acknowledgments

This work has been conducted within the framework of a technology transfer (Ko BTFSW) project and NPI activity (NPI-453) between the European Space Agency (ESA) and the Helmholtz-Zentrum Geesthacht (HZG) GmbH.

References

Buffa, G., Fratini, L., Arregi, B., Penalva, M., 2010a. A new friction stir welding based technique for corner fillet joints: Experimental and numerical study. Int. J. Mater. Form. 3, 1039–1042. doi:10.1007/s12289-010-0948-0

Cabibbo, M., McQueen, H.J., Evangelista, E., Spigarelli, S., Di Paola, M., Falchero, A., 2007. Microstructure and mechanical property studies of AA6056 friction stir welded plate. Mater. Sci. Eng. A 460, 86–94. doi:10.1016/j.msea.2007.01.022

Çam, G., Mistikoglu, S., 2014a. Recent developments in friction stir welding of al-Alloys. J. Mater. Eng. Perform. 23, 1936–1953. doi:10.1007/s11665-014-0968-x

CHEN, P.S., Bhat, B.N., 2002a. Time-Temperature-Precipitation Behavior in Al-Li Alloy 2195, Technical Report.

Chen, Z.W., Pasang, T., Qi, Y., 2008. Shear flow and formation of Nugget zone during friction stir welding of aluminium alloy 5083-O. Mater. Sci. Eng. A 474, 312–316. doi:10.1016/j.msea.2007.05.074

Colligan, K., 1999. Material Flow Behavior during Friction Stir Welding of Aluminum. Weld. J. 78, 229–237.

Gao, C., Zhu, Z., Han, J., Li, H., 2015a. Correlation of microstructure and mechanical properties in friction stir welded 2198-T8 Al–Li alloy. Mater. Sci. Eng. A 639, 489–499. doi:10.1016/j.msea.2015.05.038

J.A.Schneider, A.C.Nunes, M.S.Brendel, 1991. The Influence of Friction Stir Weld Tool Form and Welding Parameters on Weld Structure and Properties : Nugget Bulge in Self- Reacting Friction Stir Welds The Influence of Friction Stir Weld Tool Form and Welding Parameters on Weld Structure and Propertie, in: 8th International Symposium on Friction Stir Welding.

Jo, H.-H., Hirano, K., 1987. Precipitation processes in Al-Cu-Li alloy studied by DSC. Mater. Sci. Forum 13–14.

Krishnan, K.N., 2002b. On the formation of onion rings in friction stir welds. Mater. Sci. Eng. A 327, 246–251. doi:10.1016/S0921-5093(01)01474-5

Liu, H.J., Fujii, H., Maeda, M., Nogi, K., 2003a. Tensile properties and fracture locations of friction-stir-welded joints of 2017-T351 aluminum alloy. J. Mater. Process. Technol. 142, 692–696. doi:10.1016/S0924-0136(03)00806-9

Liu, H.J., Li, J.Q., Duan, W.J., 2013a. Friction stir welding characteristics of 2219-T6 aluminum alloy assisted by external non-rotational shoulder. Int. J. Adv. Manuf. Technol. 64, 1685–1694. doi:10.1007/s00170-012-4132-1

Ma, Y.E., Xia, Z.C., Jiang, R.R., Li, W., 2013b. Effect of welding parameters on mechanical and fatigue properties of friction stir welded 2198 T8 aluminum–lithium alloy joints. Eng. Fract. Mech. 114, 1–11. doi:10.1016/j.engfracmech.2013.10.010

Mishra, R.S., Ma, Z.Y., 2005a. Friction stir welding and processing. Mater. Sci. Eng. R Reports 50, 1–78. doi:10.1016/j.mser.2005.07.001

Niedzinski, M., Thompson, C., 2010b. Airware 2198 Backbone of the Falcon Family of SpaceX Launchers. Light Met. Age 68, 6–7.

Pickens, J.R., Tack, W.T., 1995. US5455003.

Prangnell, P.B., Heason, C.P., 2005b. Grain structure formation during friction stir welding observed by the "stop action technique." Acta Mater. 53, 3179–3192. doi:10.1016/j.actamat.2005.03.044

Reimann, M., Gartner, T., Suhuddin, U., Göbel, J., dos Santos, J.F., 2016. Keyhole closure using friction spot welding in aluminum alloy 6061–T6. J. Mater. Process. Technol. 237, 12–18. doi:10.1016/j.jmatprotec.2016.05.013

Scupin, P., 2015b. Semi-Stationary Shoulder Bobbin Tool (S 3 BT): A New Approach in High Speed Friction Stir Welding.

Skinner, M., Edwards, R.L., 2003b. Improvements to the FSW Process Using the Self-Reacting Technology. Mater. Sci. Forum 426–432, 2849–2854. doi:10.4028/www.scientific.net/MSF.426-432.2849

Taylor, P., Geuser, F. De, Malard, B., 2014b. Microstructure mapping of a friction stir welded AA2050 Al – Li – Cu in the T8 state 37–41. doi:10.1080/14786435.2014.887862

The Aluminum Association, 2009. International Alloy Designations and Chemical Composition Limits for Wrought Aluminum and Wrought Aluminum Alloys. VA.

Wang, F.F., Li, W.Y., Shen, J., Hu, S.Y., dos Santos, J.F., 2015c. Effect of tool rotational speed on the microstructure and mechanical properties of bobbin tool friction stir welding of Al–Li alloy. Mater. Des. 86, 933–940. doi:10.1016/j.matdes.2015.07.096

Wanhill, R.J.H., 2013c. Aerospace Applications of Aluminum-Lithium Alloys, Aluminum-Lithium Alloys: Processing, Properties, and Applications. Elsevier Inc. doi:10.1016/B978-0-12-401698-9.00015-X

Widener, C.A., Talia, J.E., Tweedy, B.M., Burford, D.A., 2006. High-Rotational Speed Friction Stir Welding ‰ With A Fixed Shoulder, in: 6th International Friction Stir Welding Symposium.

Wu, H., Chen, Y.-C., Strong, D., Prangnell, P., 2015d. Stationary shoulder FSW for joining high strength aluminum alloys. J. Mater. Process. Technol. 221, 187–196. doi:10.1016/j.jmatprotec.2015.02.015

Zhang, S., Zeng, W., Yang, W., Shi, C., Wang, H., 2014c. Ageing response of a Al–Cu–Li 2198 alloy. Mater. Des. 63, 368–374. doi:10.1016/j.matdes.2014.04.063